The Effects of Rotor-Rotor and Rotor-Wing Interactions on eVTOL Aeroacoustics

Brendan Smith PhD Student
Ullhas Udaya Hebbar PhD Student
Dr. Farhan Gandhi Redfern Chair, Director

Center for Mobility with Vertical Lift (MOVE)
Rensselaer Polytechnic Institute
Troy, New York

ABSTRACT

This study examines the effect of aerodynamic interactions on a two-rotor pair in cruise, and a propeller acting in the presence of a wing. The two-rotor system with a forward and an aft rotor in-line is considered at different disk loadings (6, 8, 12 lb/ft^2) for a fixed cruise speed and different cruise speeds (20, 40, 60 knots) for a fixed disk loading. Loads for these rotors are generated using the CFD solver AcuSolve to capture the aerodynamic interactions on the rear rotor due to the front rotor. These loads are used as inputs to an acoustic solver (PSU-WOPWOP, ANOPP2) to predict noise at observers in the rotor plane, with noise compared to that from isolated rotors in the absence of aerodynamic interactions, to quantify the interaction effects. The rotor wing case, with the rotor in front of the wing operating in axial propeller mode, is simulated at 24 knots cruise and 8° wing angle of attack. Loads for the rotor with a wing and a rotor acting in isolation are generated using the CFD solver AcuSolve. These loads are used as inputs to an acoustic solver, with observers placed in the plane of the rotor, in the plane containing the wing chord cut through the rotor hub, and a vertical plane through the hub in the wind direction. The two-rotor system simulation results show that the presence of aerodynamic interactions on the rear rotor results in changes in noise levels of less than 2 dB in the plane of the rotors. The rotor wing results show that the aerodynamic interactions increase the overall noise by up to 8 dB, with the largest increase being above and behind the prop-rotor.

1. INTRODUCTION

The ever increasing viability of distributed electric propulsion at larger and larger scales has led to increased interest in the development of electric VTOL (eVTOL) aircraft. Small-scale platforms have been in use for recreational purposes for years in tasks such as videography. The increasingly more viable large-scale platforms are being considered for new tasks such as transportation of people and goods in urban and suburban areas, as depicted in the visions laid out by the NASA UAM Grand Challenge (Ref. 1). These new tasks introduce new challenges, with a key challenge being the community acceptance of the noise generated by the eVTOL aircraft which will now be operating in areas of high population density.

Decades of research have led to a comprehensive understanding of the noise generated by conventional single main helicopters. Ref. 2 details key noise sources for conventional helicopters – thickness noise, loading noise, high speed impulsive noise, blade-vortex interaction noise, and broadband noise – and the conditions in which these sources dominate. However, a similar level of understanding for eVTOL aircraft has yet to be achieved, as although the types of noise sources remain the same, their relative importance changes.

Several groups have addressed the gap in understanding for eVTOL noise. NASA Langley Research Center (LaRC) has focused on experimental and simulation studies for small, fixed-pitch, variable RPM rotors, investigating the effects of rotor-airframe interactions, contributing noise sources, and the importance of broadband noise (Refs. 3-6). Broadband noise, a noise source not typically deemed important for traditional helicopters, has been highlighted as a particularly important noise source for eVTOL rotors by Intaratep et. al (Ref. 7), with many groups investigating broadband noise for a variety of UAM platforms (Refs. 5, 8-10). Passe and Baeder identified key parameters in noise reduction, such as number of blades and tip speed, for larger scale rotor designs more typical of UAM missions. Gandhi et al. examined how changing rotor solidity through increasing chord and number of blades while holding the disk loading constant changed the acoustic signature of a rotor (Ref 11). There have also been investigations into the possibility of using rotor phase control to achieve acoustic benefits, as many eVTOL aircraft propose pairs of rotors in close proximity. Schiller et al. looked at the cancellation effects of rotor pairs and then applied these to an octocopter to examine the noise benefits at a vehicle level (Ref. 12). Pascioni et al. were able to use directivity patterns

Presented at the Vertical Flight Society's 79th Annual Forum & Technology Display, West Palm Beach, FL, May 16-18, 2023

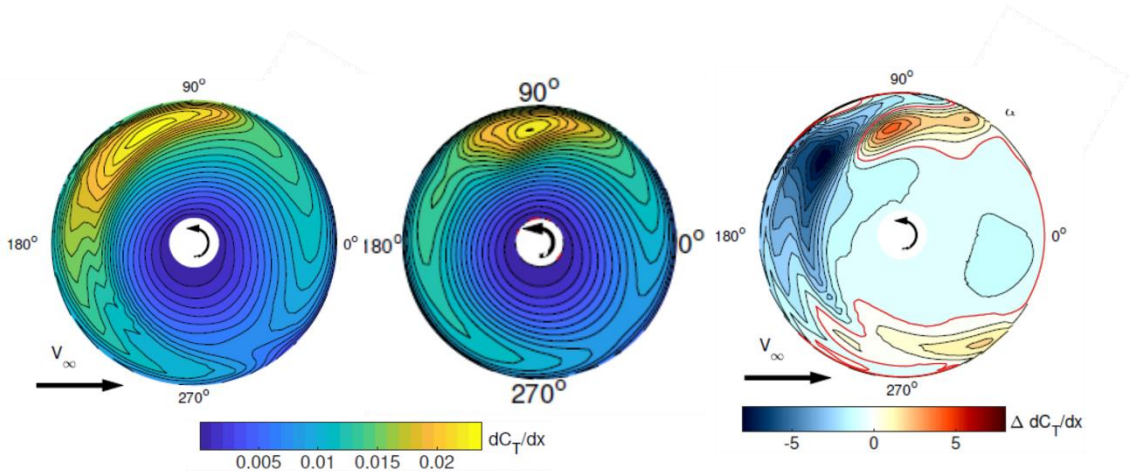

Figure 1 – For 6 lb/ft^2 40 Knots Cruise Isolated rear rotor sectional thrust coefficient (left) rear rotor sectional thrust coefficient in the presence of a front rotor (center), and difference in sectional thrust coefficient between rear rotor in presence of interactions and isolated rear rotor (right)

generated by relative propeller phase to create targeted regions of quiet noise for a distributed propulsion VTOL concept (Ref. 13). Smith et al. investigated how the noise of a quadcopter, hexacopter, and octocopter are changed with adjacent rotors perfectly in and out of phase, and then looked at the case for rotors out of phase in forward flight (Ref. 14, 15).

Many proposed designs call for multiple rotors operating in close proximity to one another, or rotors operating as propellers in close proximity to wings. These conditions lead to aerodynamic interactions that impact the aerodynamic loads, and subsequently the acoustics generated by the aircraft. To address this, studies have looked at the interactional effects on aerodynamics and aeroacoustics using Vortex Particle Methods (VPM) and CFD for side-by-side as well as stacked rotor configurations (Refs. 8, 16, 17). Additionally, Penn State detailed a case of two propellers acting near wings and how the aerodynamic interactions changed the noise signature (Ref. 18). Smith et al. looked at how aerodynamic interactions from the ground affected the noise that were produced by a rotor pair and how it compared to isolated rotors (Ref. 19).

Although studies have investigated the effects of rotor-rotor and propeller-wing interactions on acoustics, there are still many conditions and vehicle scales to be investigated. This study looks to increase the knowledge in these areas by looking at an in-line rotor pair in cruise to examine how the front rotor's aerodynamic effects on the rear rotor change the acoustics of the two-rotor system, and how the acoustics of a rotor operating as a propeller in front of wing compare to an isolated rotor under the same conditions.

2. ANALYSIS

2.1 Two-Rotor System in Forward Flight Analysis

The airloads for a two-rotor assembly in cruise are generated using CFD as described in Ref 20. The rotors are 2-bladed, 5.5 ft diameter Whirlwind propellers with a fixed hub-to-hub separation of 3 rotor radii, with 60° phasing between the pair. Due to the rotors being aligned in the direction of the flow, the wake of the front rotor influences the aerodynamics of the rear rotor, changing the thrust over the aft rotor disk as demonstrated in Figure 1. The rotor pair is considered at different disk loadings (6 lb/ft^2, 8 lb/ft^2, and 12 lb/ft^2) for a fixed forward flight speed of 40 knots and at different forward flight speeds (20 knots, 40 knots, and 60 knots) for a fixed disk loading of 6 lb/ft^2 as variation in operating conditions affect the interactional aerodynamic effects on the rear rotor. To examine the acoustic effects of interactional aerodynamics, two separate acoustic simulations are run: a case with a rear rotor in isolation and a case with a rear rotor affected by the presence of the front rotor.

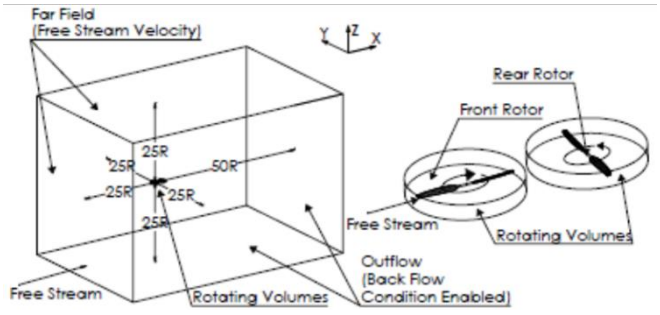

Figure 2 – Two rotor system CFD computation domain

The CFD simulations are conducted using the commercial Navier-Stokes solver AcuSolve which uses a

stabilized 2nd order upwind finite element method. AcuSolve simulations for a Straight Up Imaging (SUI) Endurance rotor were previously shown to compare well against experimental results (Ref. 21). The computational domain for the two-rotor assembly is shown in Figure 2. The nonrotating volume is a rectangular prism with the incoming freestream side and top set to Far Field and the remaining sides and bottom set to outflow with backflow conditions enabled. Around each rotor is a cylindrical rotating volume with interface surfaces that pass information to and from the non-rotating volume. A full description of the CFD methodology details can be found in Ref. 20.

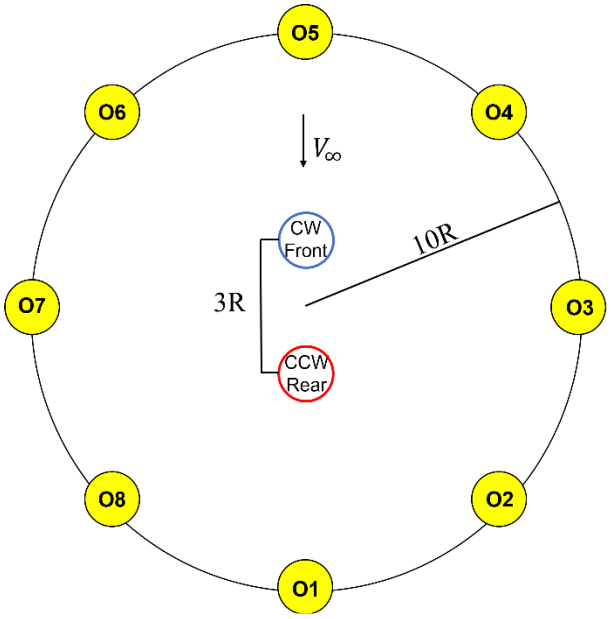

Figure 3 – Setup of two-rotor system and 8 observer locations

Two different acoustic solvers are used, PSU-WOPWOP (Ref. 22) and ANOPP2 (Ref. 23), both of which are based on the numerical implementation of Farassat's Formulation 1A of the Ffowcs Williams and Hawkings (FW-H) equation. Both were used and yielded the same tonal noise predictions for the same rotor loading. Broadband noise predictions are obtained using ANOPP2 which has previously shown good validation with experiments for broadband noise of small electrically powered rotors (Ref. 5). Chordwise compact loads from CFD are provided to the acoustic solver to compute the discrete frequency (tonal) noise from thickness and loading sources. The solver calculates acoustic pressure time history at chosen observer locations selected by the user, with pressure coming from a specified number of rotors (whose position and relative phasing are specified). The observers chosen for the two-rotor system are shown in Figure 3, with 8 observers placed in-plane with the rotors in a circle of 10 rotor radii centered on the rotor pairing, giving observers placed at 45° increments in azimuth. An overall noise prediction at each

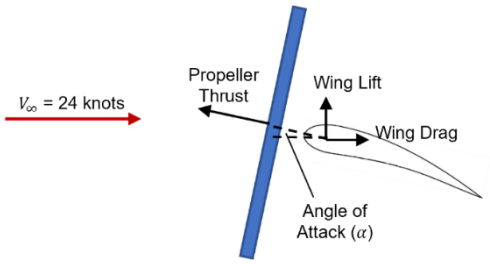

Figure 4 – Side view of propeller wing setup

observer is obtained by combining the tonal noise predictions with the broadband predictions in the frequency domain.

2.2 Propeller-Wing Assembly Analysis

The airloads for the rotor-wing assembly are generated using CFD as described in Ref 23. The assembly is based on the Army Research Laboratory's quadrotor bi-plane CRC-20. The CRC-20 is a quad-rotor biplane with a blown wing configuration (Ref. 24). The ALM-based CFD simulation for the rotor-wing interaction uses a half-wing unit of the CRC-20 with one rotor simulated as an infinite co-rotating rotor-blown wing by employing a periodic boundary condition in the wing-spanwise directions. The 24 inch diameter rotor is located at the center of the half-wing unit and 2.75 inches upstream of the leading edge of the 30 inch span half-wing. The wing comprises an untapered and untwisted Wortmann FX 63-137 airfoil with a 10 inch chord while the rotor is a scaled up version of the two-bladed straight-up imaging (SUI) endurance rotor (Ref. 27). The rotor-axis is aligned with the wing chord and the rotor-wing unit is simulated for an 8° wing angle-of-attack (AOA), a freestream velocity of 24 kts and a counter-clockwise rotational speed of 2900 RPM for the rotor. A side view of the rotor-wing configuration is shown in Figure 4.

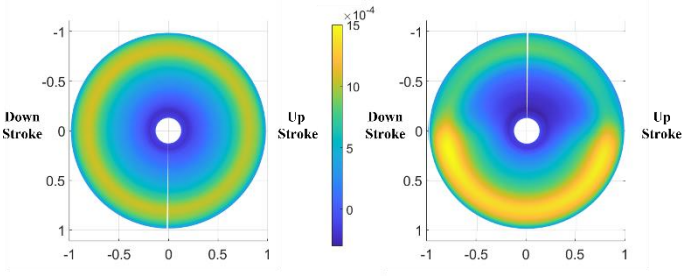

Figure 5 – Disk plots of sectional thrust coefficient for rotor (left) in isolation (right) with

The ALM-based rotor-wing interaction CFD simulation employs a delayed detached eddy simulation (DDES) model. Briefly, the Spalart-Allmaras (SA) turbulence model is employed near the wing while a static large eddy simulation (LES) type sub grid-scale model is used away from the wing.

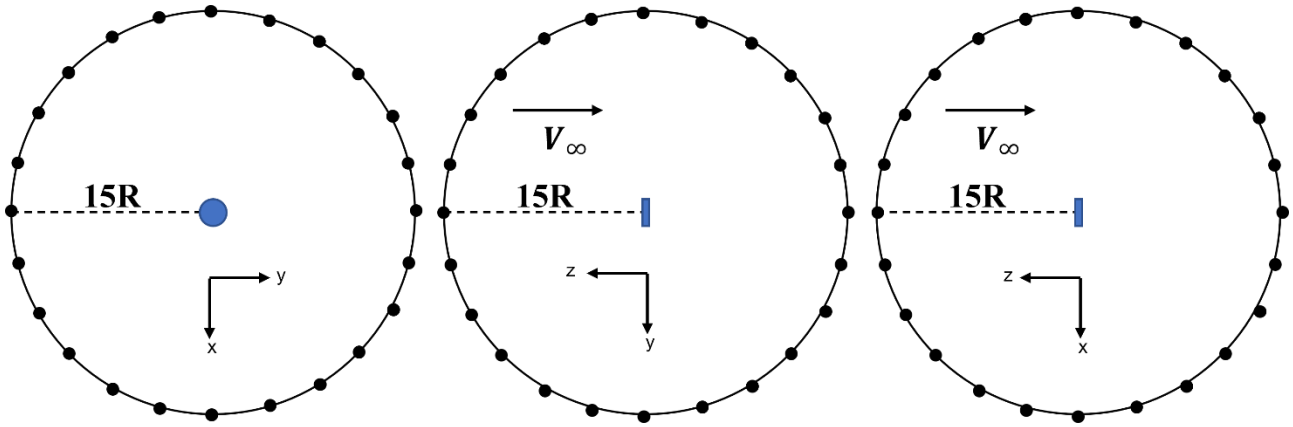

Figure 6 – Observers in plane of rotor (left), plane containing wing chord cut through the rotor hub (center), and vertical plane through the hub in the direction of the wind (right)

A boundary layer transition model (specifically the γ model) is also used to better model the transition of the wing boundary layer to turbulence. The DDES simulations are performed on the commercial Navier-Stokes solver, AcuSolve.

The actuator-line method (ALM) models the propeller blades by introducing time-varying momentum sources in the Navier-Stokes equations, essentially representing the motion of the rotor blades. The method utilizes sampling of the induced velocities around the rotor and subsequently employing airfoil tables (lift and drag coefficients vs. local AOA) to arrive at blade-span varying lift and drag values consistent with the induced velocities. Smearing kernels are employed in the rotor-normal and tangential directions to distribute the computed loads about a width of $c_r = 2.42$ inches corresponding to the characteristic blade chord; this is necessary to avoid numerical instabilities. The solver is restricted to a 2° timestep for the rotation of the actuator lines to ensure accuracy. More details regarding ALM, meshing, and problem setup for this simulation is available in Refs. 23 and 26.

A disk plot showing the sectional lift coefficient for the isolated and interactional rotors is shown in Figure 5. The isolated case is mostly axisymmetric, with only slight increase in lift coefficient on the downstroke side as some of the flow is acting in the plane of the rotor due to the 8° AoA causing an advancing and retreating side effect on the rotor thrust distribution. The interactional case shows asymmetry in the vertical direction, with more thrust accumulating below the wing in the bottom of the disk, and less thrust along the top of the disk. Like the isolated case, there is slightly greater accumulation of thrust on the downstroke side of the disk as compared to the upstroke side. The difference in thrust over the top and bottom half of the disk due to the wing results in decrease in thrust of 3.3%, meaning the aerodynamic interactions due to a wing cause an overall thrust. But, the region of increased lift across the bottom of the rotor disk results in an increase in the peak sectional thrust value by 38.4%.

Similar to the two-rotor system, the CFD loads are provided to an acoustic solver to predict acoustic pressure time history at chosen observers. The observers are arranged in circles of 15 rotor radii in the plane of the rotor, in the plane containing the wing chord cut through the rotor hub, and a vertical plane through the hub in the wind direction as shown in Figure 6. Each circle of observers is centered on the rotor hub and contain 24 observers, giving noise every 15°. Acoustic predictions for the rotor acting in the presence of a wing are compared to the isolated rotor to understand how the presence of aerodynamic interactions due to the wing change the acoustics of the rotor.

3. RESULTS

3.1 Two-Rotor System at Constant Cruise Speed

This section focuses on the two-rotor system at a constant 40 knots cruise with increasing disk loading (6 lb/ft^2, 8 lb/ft^2, and 12 lb/ft^2). Beginning with the 6 lb/ft^2 case, in which the aft rotor produces 11.5% less thrust in the presence of a front rotor, the overall sound pressure level (OASPL) at the 8 observers (shown in Figure 3) is given in Tables 1a and 1b, with Table 1a containing the noise for the isolated pair and Table 1b containing the noise for the case with aerodynamic interactions. The noise is broken into tonal noise, broadband noise, and the overall noise which accounts for both. Beginning with a comparison of the broadband noise, the interactional rotor pair consistently produces ~1dB more of broadband noise at all observers, with a maximum difference of 1.3 dB at observer 5, directly in front of the rotor pair.

Tables 1a and 1b – 6 lb/ft^2 40 knots cruise OASPL at observers for (**a**: left) isolated rear rotor, and (**b**: right) interactional rear rotor

Observer	Tonal Noise (dB)	Broadband Noise (dB)	Overall Noise (dB)
1	75.60	61.02	75.75
2	82.78	61.72	82.82
3	86.56	63.33	86.58
4	83.80	66.21	83.87
5	92.20	67.21	92.21
6	90.0	65.14	90.01
7	85.16	63.28	85.19
8	77.85	61.71	77.95

Observer	Tonal Noise (dB)	Broadband Noise (dB)	Overall Noise (dB)
1	75.38	61.12	75.58
2	82.39	62.88	82.44
3	85.87	64.56	85.91
4	83.22	67.16	83.33
5	91.96	68.54	91.98
6	89.74	66.21	89.76
7	84.70	64.46	84.74
8	75.80	62.84	76.01

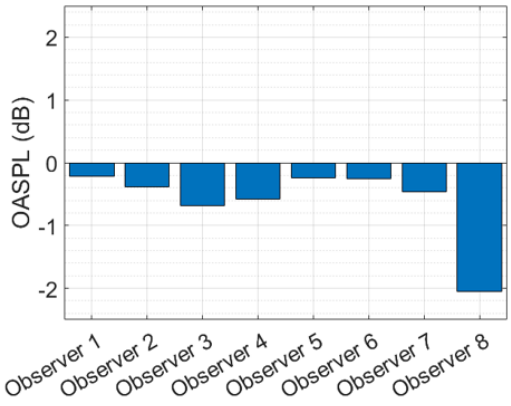

Figure 7 – 6 lb/ft^2 40 knots cruise difference plot of tonal noise OASPL (Interaction – Isolated)

Tonal noise differences vary, so a visual comparison of the difference between the isolated and interactional cases is given in Figure 7. This reveals that the presence of aerodynamic interactions decreases tonal noise across all observers, and at most decreases the noise by 2 dB at observer 8. Among the remaining observers (1-7) the noise difference is minimal, decreasing by less than 0.7 dB, with a maximum difference at observer 3. The general noise decrease is caused by the reduction in loading on the rear rotor, as shown in Figure 1, and as such the loading noise is reduced resulting in a general decrease in tonal noise. It should be noted that although the interaction case sees an increase in the broadband noise, the magnitude of noise is much lower than the tonal noise and as such the increase is insignificant to the overall noise comparison shown in Tables 1a and 1b. Overall, the change in noise due to the aerodynamic interactions from the front rotor wake are small, with an average change in noise of 0.6 dB.

This comparison is further examined by looking at the difference in acoustic pressure time history for the isolated and interactional cases. Figure 8 shows this comparison in tonal noise at observer 3, with the rear rotor loading pressure for the isolated and interaction case shown, along with the total noise from both rotors and the sound pressure level (SPL) as a function of frequency. The front rotor loading noise comparison is excluded as the interactional effects only impact the rear rotor. The comparison of rear rotor loading noise reveals the only difference to be a slight decrease in magnitude of the signal when aerodynamic interactions are considered. There is no impact on the phase or periodicity of the signal, and as a result when the noise from both rotors is considered the overall pressure signal varies only slightly in magnitude, which is reflected in the 0.69 dB difference in tonal noise shown at observer 3. The SPL plot reinforces this, showing similar magnitude peaks at the 2/rev, 4/rev, 6/rev, and frequencies. There is some difference in high frequency peaks, but these peaks sit at magnitudes well below that of the dominant tonal peaks.

The next comparison looks at the rotor pairing with an increased disk loading of 8 lb/ft^2 with the same cruise speed of 40 knots. As detailed in Ref. 20, an increase in the disk loading causes a decrease in the aerodynamic interactions on the rear rotor due to the front rotor. This is due to the front rotor wake convecting downwards at a lower wake skew angle as disk loading increases, thus reducing the interactional effects with the rear rotor. For the 8 lb/ft^2 case, this means that the rear rotor in the presence of a front rotor produces 10% less thrust as compared to the 11.5% less thrust for the previous 6 lb/ft^2. The noise at the 8 observers for the isolated and interactional cases at 8 lb/ft^2 is given in Tables 2a and 2b respectively. Beginning with the broadband noise comparison, the results look similar to what were seen at 6 lb/ft^2, with the interactional case showing an increase in broadband noise at all observers with a maximum increase of 1.5 dB at observer 4. Tonal noise comparisons also look similar, with the difference plot given in Figure 9. Unlike the 6 lb/ft^2 case, observer 1 exhibits an increase in noise when aerodynamic interactions are considered, with an increase of 1.13 dB. But, the tonal noise between isolated and interactional rear rotors is within ~1dB, with most observers exhibiting lower noise for the interactional case with a max reduction of 1.04 dB at observer 8. And when looking at the average absolute noise difference, the average sits lower for 8 lb/ft^2 at 0.49 dB compared to the 0.6 dB for 6 lb/ft^2 showing that the weaker

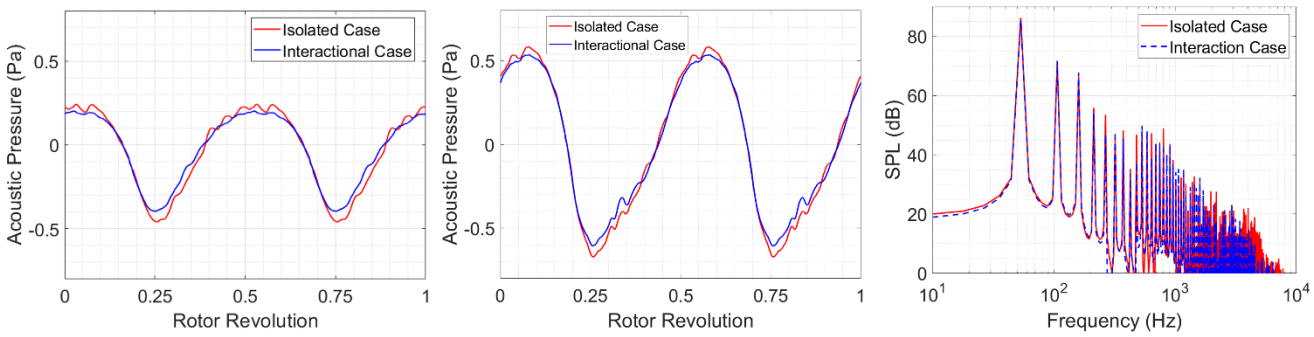

Figure 8 – 6 lb/ft^2 40 knots cruise observer 3 rear rotor loading noise acoustic pressure time history (left), two-rotor system overall tonal noise acoustic pressure time history (center), and SPL as a function of frequency (right)

Tables 2a and 2b – 8 lb/ft^2 40 knots cruise OASPL at observers for (**a**: left) isolated rear rotor, and (**b**: right) interactional rear rotor

Observer	Tonal Noise (dB)	Broadband Noise (dB)	Overall Noise (dB)
1	79.58	63.74	79.69
2	87.18	64.39	87.20
3	89.55	65.86	89.57
4	88.57	68.54	88.61
5	96.62	68.57	96.63
6	92.36	67.54	92.37
7	88.02	65.81	88.05
8	80.14	64.37	80.25

Observer	Tonal Noise (dB)	Broadband Noise (dB)	Overall Noise (dB)
1	80.71	64.79	80.82
2	86.97	65.51	87.0
3	88.95	67.09	88.98
4	88.20	70.04	88.27
5	96.36	69.56	96.37
6	92.24	68.63	92.26
7	87.80	67.0	87.83
8	79.10	65.46	79.28

aerodynamic interactions bring the tonal noise between the two cases even closer together.

A comparison of the acoustic pressure time history and SPL for the 8 lb/ft^2 case at observer 3 is given in Figure 10. Similar to what was found for 6 lb/ft^2, the loading noise from the rear rotor has similar shape and frequency content, with only a slight change in magnitude. This is reflected in the overall noise signal, resulting in the 0.6 dB noise difference shown in Figure 9. The frequency content shown in the SPL is also similar between the isolated and interactional cases, with the 2/rev, 4/rev, 6/rev, and 8/rev peaks at similar magnitudes, and again the minor differences at higher frequencies sit at magnitudes well below the dominant tonal peaks and are thus insignificant.

The final comparison at 40 knots cruise is for a disk loading of 12 lb/ft^2, with the noise comparisons given in Tables 3a and 3b. As discussed earlier, a further increase in disk loading causes a further decrease in the aerodynamic interactions of the front rotor on the rear rotor, with the aerodynamic interactions causing the rear rotor to produce 9.0% less thrust. As such one should expect the noise difference between the isolated and interaction cases to be the lowest of all cases. Broadband noise differences look similar to the other disk loadings with increases at all observers ~1.25 dB and a maximum of 1.46 dB at observer 3. Tonal noise

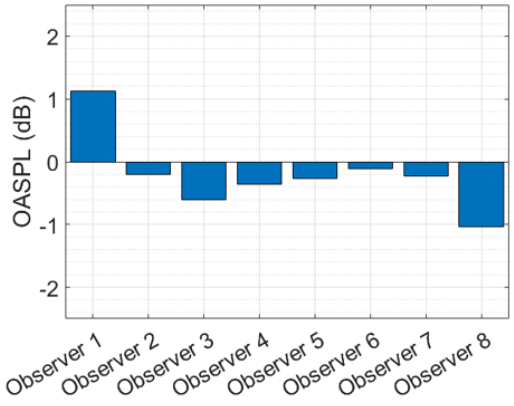

Figure 9 – 8 lb/ft^2 40 knots cruise difference plot of tonal noise OASPL (Interaction – Isolated)

comparisons are given in Figure 11. Comparing these differences to those observed for 6 lb/ft^2 and 8 lb/ft^2, the differences between the interactional and isolated cases are lower. This is due to the even weaker aerodynamic interactions for the 12 lb/ft^2 disk loading pair, with the average absolute difference being 0.25 dB, which is lower than the 0.49 dB for 8 lb/ft^2 and 0.6 dB for 6 lb/ft^2. Across all disk loadings, the presence of interactional aerodynamics at 40

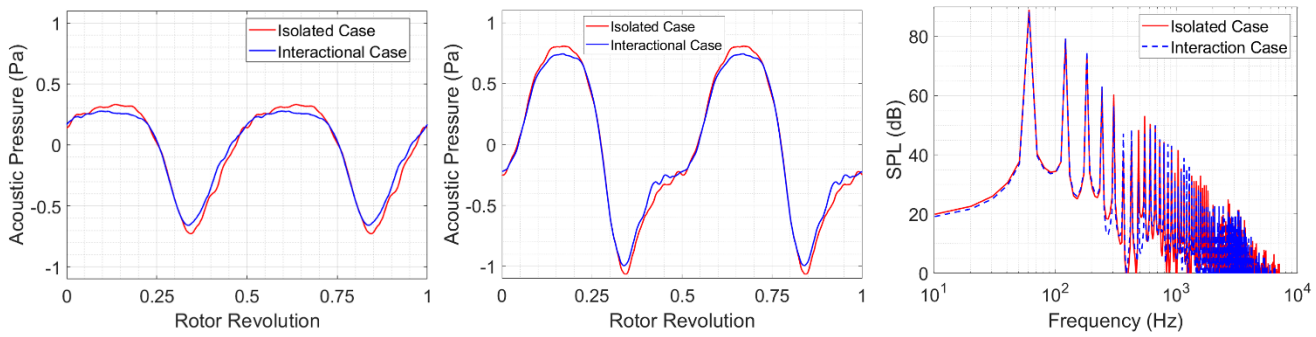

Figure 10 – 8 lb/ft^2 40 knots cruise observer 3 rear rotor loading noise acoustic pressure time history (left), two-rotor system overall tonal noise acoustic pressure time history (center), and SPL as a function of frequency (right)

Tables 3a and 3b – 12 lb/ft^2 40 knots cruise OASPL at observers for (**a**: left) isolated rear rotor, and (**b**: right) interactional rear rotor

Observer	Tonal Noise (dB)	Broadband Noise (dB)	Overall Noise (dB)
1	88.93	67.39	88.97
2	92.37	67.98	92.38
3	94.20	69.42	94.21
4	95.93	70.75	95.94
5	101.88	71.80	101.89
6	97.09	71.20	97.10
7	93.20	69.34	93.22
8	86.85	67.95	86.91

Observer	Tonal Noise (dB)	Broadband Noise (dB)	Overall Noise (dB)
1	89.68	68.72	89.71
2	92.25	69.39	92.27
3	93.86	70.88	93.88
4	95.80	72.06	95.82
5	101.69	72.91	101.70
6	96.93	72.37	96.95
7	93.19	70.72	93.22
8	87.15	69.31	87.22

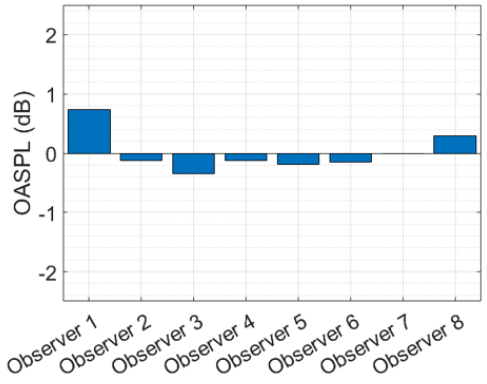

Figure 11 – 12 lb/ft^2 40 knots cruise difference plot of tonal noise OASPL (Interaction – Isolated)

knots cruise proved to have little impact on the noise emitted by the rotor pair, reducing the OASPL up to a maximum of 2.1 dB (6 lb/ft^2 observer 8) and causing very little change in the pressure signals and frequency content.

3.2 Two-Rotor System at Constant Disk Loading

The next set of comparisons look at the 6 lb/ft^2 disk loading rotor-pair at different cruise speeds, with the cruise speed slowed down to 20 knots and increased to 60 knots. Ref. 20 details that as the cruise speed increases and the rotor wake skew angle increases, the rear rotor experiences stronger aerodynamic interactions. This results in the 20 knots cruise speed condition having the least interactional effects, with the rear rotor producing 5.4% less thrust, and 60 knots cruise speed having the most interactional effects, with the rear rotor producing 12.2% less thrust. For the 20 knots cruise speed, the noise at each observer for the isolated and interaction cases is given in Tables 4a and 4b, with noise broken down into tonal, broadband, and overall noise. Broadband noise at 20 knots cruise exhibits a similar trend as to what was exhibited at 40 knots cruise speed, with the interactional case producing more broadband noise at all observers. The level of increase however is smaller, with the maximum increase being only 0.69 dB at observer 1 as opposed to the 1.3 dB maximum for the 40 knots case. Still, the broadband noise magnitudes are much lower than the tonal noise magnitude and as such have little impact on the overall noise. When comparing tonal noise, from the difference plot given in Figure 12, interactional aerodynamics increases noise at observers 1, 2, and 8 with a max increase up to 1.4 dB. Smaller reductions in tonal noise are observed at the remaining observers. Overall, the weaker interactions cause the absolute average difference at all observers to be 0.49 dB, which is smaller than the 0.61 dB for 40 knots cruise, showing again that weaker interactions produce less difference in overall noise between the interactional and isolated cases.

Tables 4a and 4b – 6 lb/ft^2 20 knots cruise OASPL at observers for (**a**: left) isolated rear rotor, and (**b**: right) interactional rear rotor

Observer	Tonal Noise (dB)	Broadband Noise (dB)	Overall Noise (dB)
1	77.65	62.84	77.79
2	82.40	63.18	82.46
3	81.44	64.09	81.52
4	81.62	65.88	81.74
5	89.19	66.70	89.21
6	86.86	65.29	86.89
7	80.81	64.07	80.90
8	70.78	63.17	71.48

Observer	Tonal Noise (dB)	Broadband Noise (dB)	Overall Noise (dB)
1	78.71	63.53	78.84
2	82.54	63.85	82.60
3	80.91	64.69	81.01
4	81.58	66.33	81.70
5	88.93	67.29	88.96
6	86.66	65.77	86.69
7	80.51	64.64	80.63
8	72.18	63.82	72.77

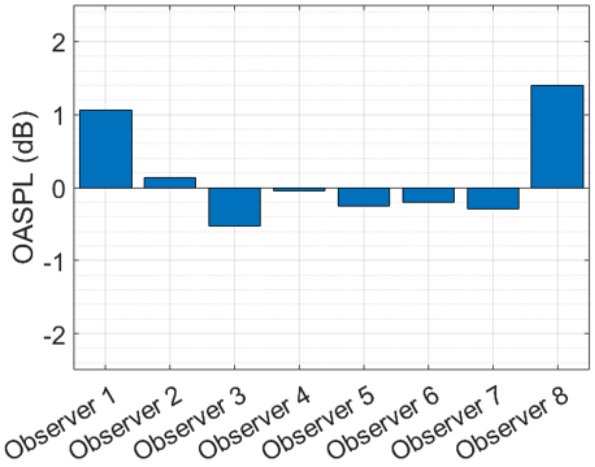

Figure 12 – 6 lb/ft^2 20 knots cruise difference plot of tonal noise OASPL (Interaction – Isolated)

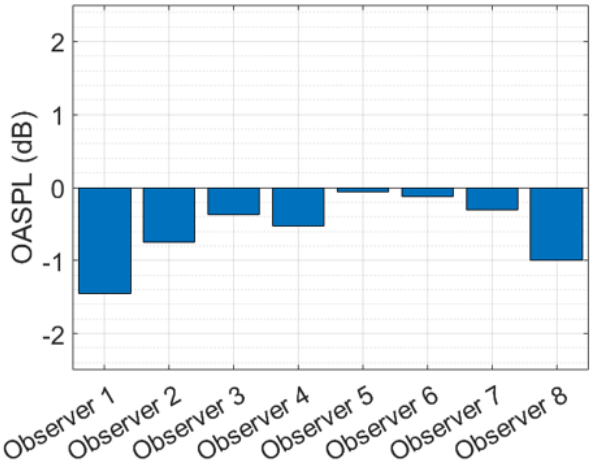

Figure 13 – 6 lb/ft^2 60 knots cruise difference plot of tonal noise OASPL (Interaction – Isolated)

Tables 5a and 5b – 6 lb/ft^2 60 knots cruise OASPL at observers for (**a**: left) isolated rear rotor, and (**b**: right) interactional rear rotor

Observer	Tonal Noise (dB)	Broadband Noise (dB)	Overall Noise (dB)
1	80.44	60.82	80.48
2	81.73	62.03	81.75
3	89.78	64.45	89.79
4	86.54	67.77	86.59
5	94.55	69.47	94.56
6	92.24	66.57	92.25
7	87.92	64.31	87.94
8	82.93	61.98	82.97

Observer	Tonal Noise (dB)	Broadband Noise (dB)	Overall Noise (dB)
1	81.88	58.99	81.91
2	82.45	60.18	82.47
3	90.15	62.62	90.16
4	87.07	66.46	87.10
5	94.61	67.62	94.62
6	92.36	65.05	92.37
7	88.23	62.55	88.24
8	83.93	60.16	83.95

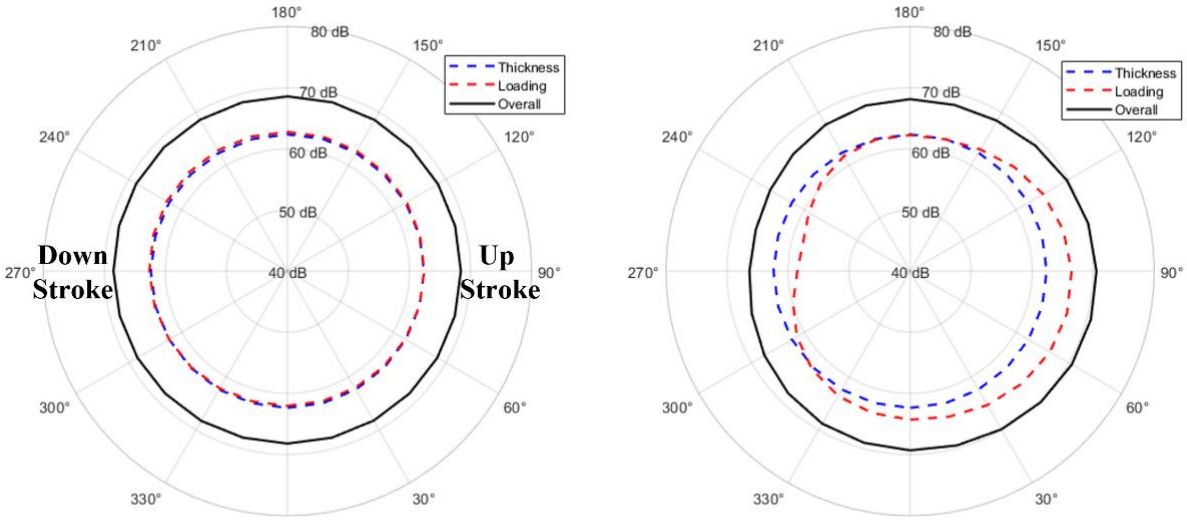

Figure 14 – OASPL noise in rotor plane for the isolated rotor (left), and rotor with wing interactions (right), as viewing from the front of the rotor

The final comparison is for the higher cruise speed of 60 knots at the same disk loading of 6 lb/ft^2, which experiences stronger aerodynamic interactions than the 20 and 40 knots cruise speeds. The noise at each observer is given in Tables 5a and 5b. Again, the broadband noise is greater for the interactional case, and at the higher cruise speed the difference is greater, with the maximum increase being 1.85 dB and the average being 1.72 dB. This increase is still not enough to cause a substantial difference in overall noise as the magnitudes are well below those of tonal noise for all observers. Looking at the difference plot in Figure 13, the tonal noise comparison exhibits similar characteristics to all cases examined so far. For all observers, the interactional aerodynamics leads to noise reductions, with a maximum difference of 1.44 dB at observer 1. The absolute average difference is 0.6 dB, which is the same as for 40 knots cruise speed. When considering all cruise speeds examined the greatest noise difference is only 2.1 dB and the greatest absolute average difference in noise is 0.6 dB. These differences are not large and demonstrate again that for a two-rotor pair in cruise the aerodynamic effect of the front rotor on the aft rotor has only a small impact on the noise produced by the rotor pair. The magnitude of reduction in noise broadly correlates to the load reduction on the aft rotor due to interactional aerodynamic effects. Although the broadband noise generally increases with interactional aerodynamics (by up to 1.85 dB) the reductions in tonal noise (dominant for the conditions considered) drive the overall reductions in noise observed.

3.3 Propeller-Wing at 8° AoA

Figure 5 previously showed the rotor loads for an isolated Trotor and a coupled rotor-wing system with interactional aerodynamic effects included. For these loading cases, Figure 14 shows the noise in the rotor plane, with noise split into thickness, loading, and overall noise. Thickness noise is the same for both cases as they use the same geometry and operate at the same rotational speed. Examining loading noise for the isolated case, the noise across all observers is similar, which is reflective of the sectional thrust coefficient shown in Figure 5 that shows mostly azimuthally independent loading. For the interactional rotor, this is no longer the case, as there is region of peak noise below the wing and on the upstroke side (Ψ = 330° - 150°) and a quieter region located above the wing on the downstroke side (Ψ = 225° - 300°). This is reflective of the sectional loading for the rotor-wing system in Figure 5, where loading is much higher across the bottom of the disk compared to the top, resulting in the development of these increased and decreased noise regions seen on Fig. 14. A direct comparison between the overall noise (sum of loading plus thickness noise) between the rotor with aerodynamic interactions and the isolated rotor is given in Figure 15, for observers at 30° increments. From the figure, it is evident that aerodynamic interactions result in an increase in noise is up to 2.23 dB on the upstroke side at (Ψ = 330° -

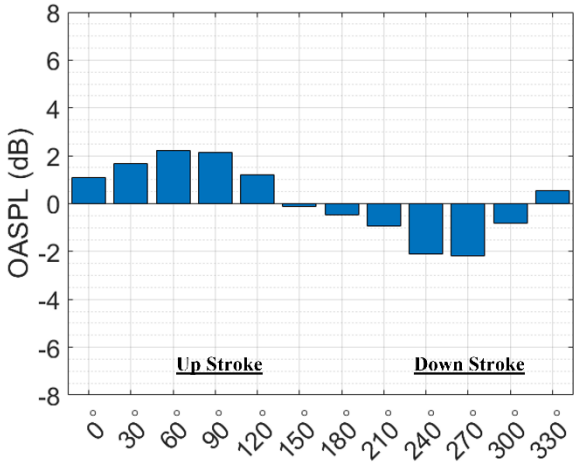

Figure 15 – OASPL difference in rotor plane (Interaction – Isolated)

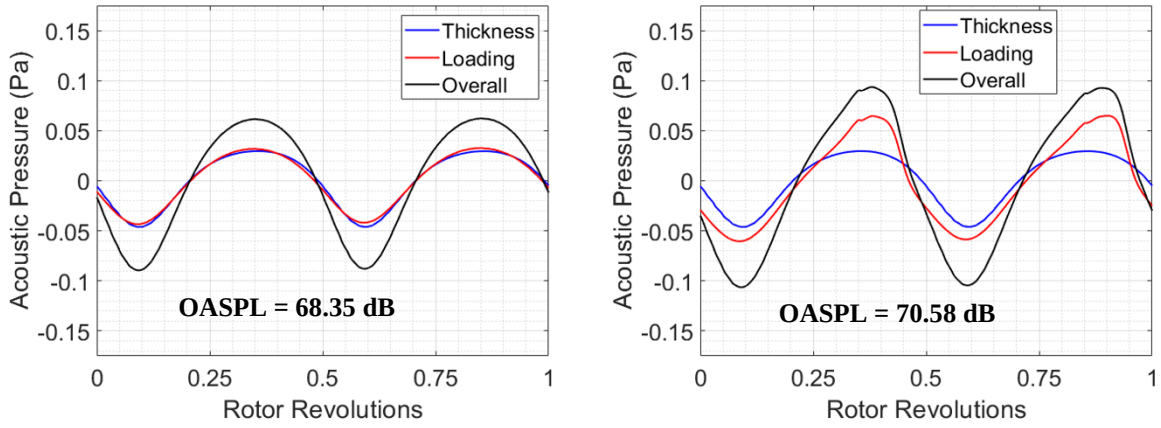

Figure 16 – Acoustic pressure time history at $\Psi = 60^{\circ}$ observer for (left) isolated rotor (right) rotor with wing interactions

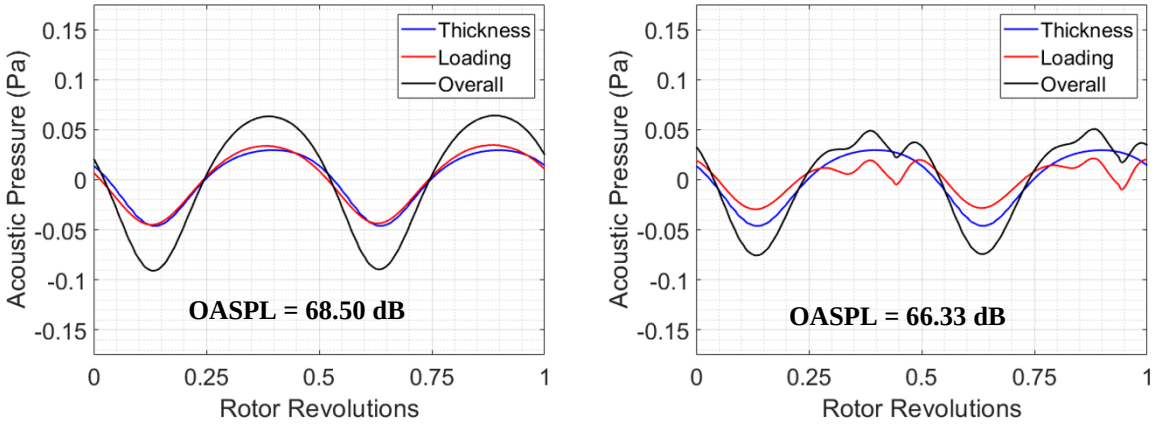

Figure 17 – Acoustic pressure time history at $\Psi = 255^{\circ}$ observer for (left) isolated rotor (right) rotor with wing interactions

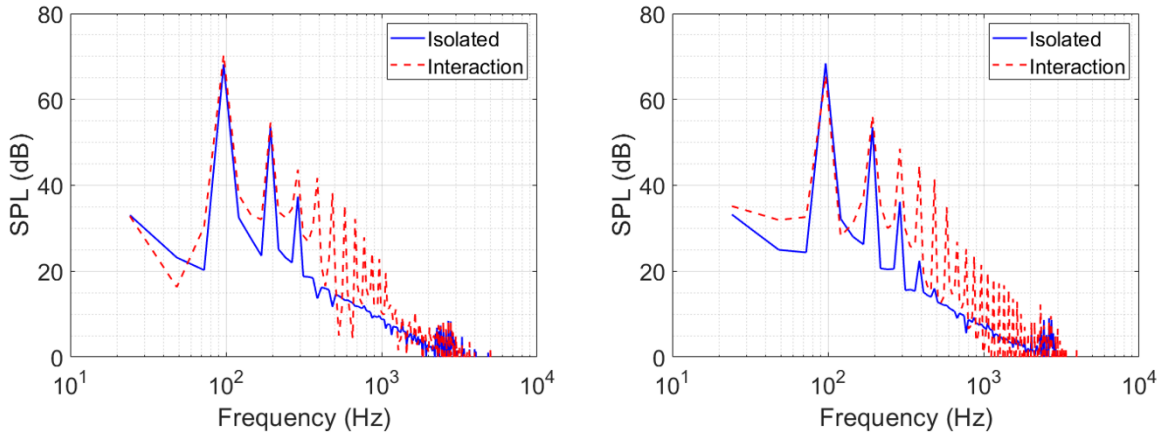

Figure 18 – Sound pressure level (SPL) vs frequency comparison of isolated and interactional propellers at (left) $\Psi = 60^{\circ}$ (right) $\Psi = 255^{\circ}$observer

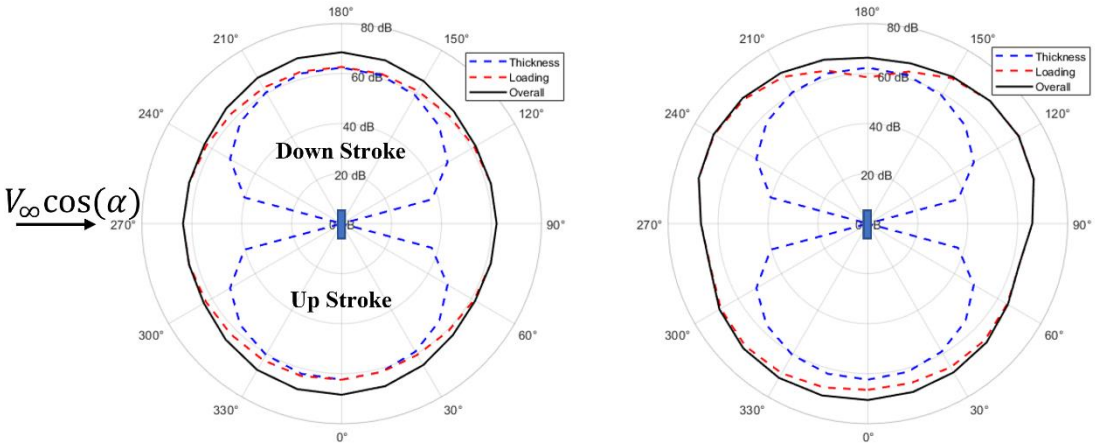

Figure 19 – OASPL noise in wing chord plane for isolated rotor (left), and rotor with wing interactions (right), as viewed from above the rotor

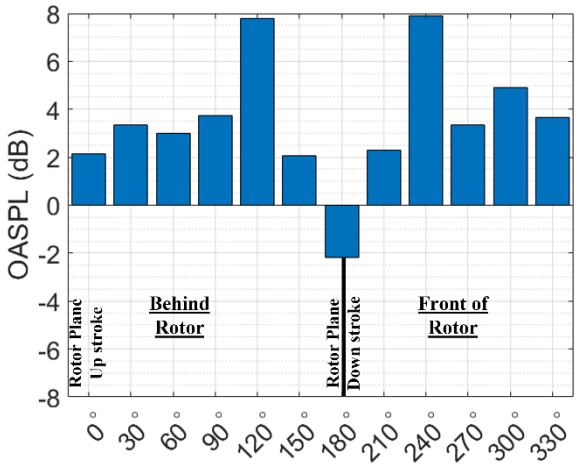

Figure 20 – OASPL difference in wing chord plane (Interaction – Isolated)

120°) and a decrease of up to 2.17 dB on the down stroke side (Ψ = 210° - 300°). But, the change in average noise across all observer locations is only a 0.22 dB increase, showing that aerodynamic interactions due to the presence of the wing does not greatly change the noise in the rotor plane.

In addition to the change in OASPL, the presence of aerodynamic interactions changes the pressure signal and frequency content of the noise. Beginning with a comparison of the acoustic pressure at Ψ = 60°, shown in Figure 16, the acoustic pressure is broken down into thickness, loading, and overall noise. The isolated case shows a 2/rev signal with a neither thickness nor loading noise as the dominant source, as was observed in the OASPL in Figure 14. The interactional case shows a change in the loading noise magnitude, with the loading noise being the dominant noise source compared to the thickness noise, with the presence of additional low frequency tones. A second comparison of the acoustic pressure is given in Figure 17, showing the acoustic pressure time history at the Ψ = 255° observer where the interactional rotor is quieter than the isolated rotor. Again, the isolated rotor shows comparable noise between the thickness and loading sources and only a slight amount of high frequency content in the noise signal. The interactional case has thickness noise as the dominant noise source instead of loading noise as the observer is located at a region of lower loading noise for the interactional case, with additional low frequency tones. To compare how the frequency content differs, the SPL vs frequency is compared in Figure 18. Starting with the Ψ = 60° observer, the comparison shows the interactional rotor having greater peaks at the 2/rev, 4/rev, and 6/rev frequencies, which is reflective of the difference in loading noise magnitude at this observer. In addition, the interactional rotor peaks at frequencies up to 20/rev, or 10 times the blade passage frequency while the isolated rotor has no peaks beyond 6/rev. These additional peaks are reflective of the additional low frequency tones observed in the pressure signal and could change the noise when considering A-weighting which biases noise towards higher frequencies that humans are more sensitive to. To examine this the difference in A-weighted noise at the Ψ = 60° observer is compared to the difference in unweighted noise. The A-weighted difference is 2.47 dBA, while the unweighted difference is 2.23 dB, showing these additional tonal peaks at higher frequencies do not change the noise even when biasing towards higher frequencies. The difference between the isolated and interactional rotor at Ψ = 255° is similar, with the interactional rotor having peaks into much higher frequencies than the isolated rotor. At this observer these peaks do cause a difference in the A-weighted noise, with the difference in unweighted noise being 2.12 dB and the difference in A-weighted noise being 0.22 dBA. So, depending on the observer the presence of interactions can

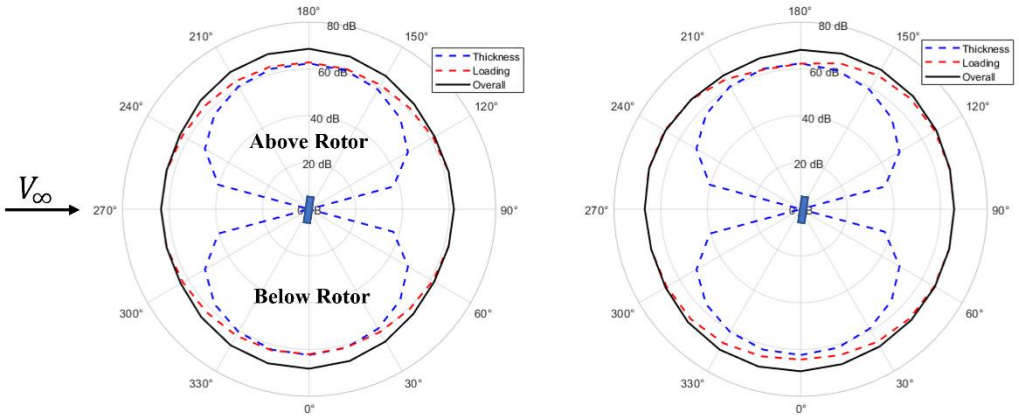

Figure 21 – OASPL noise in vertical plane in wind direction for isolated rotor (left), and rotor with wing interactions (right) as viewed from the up stroke side

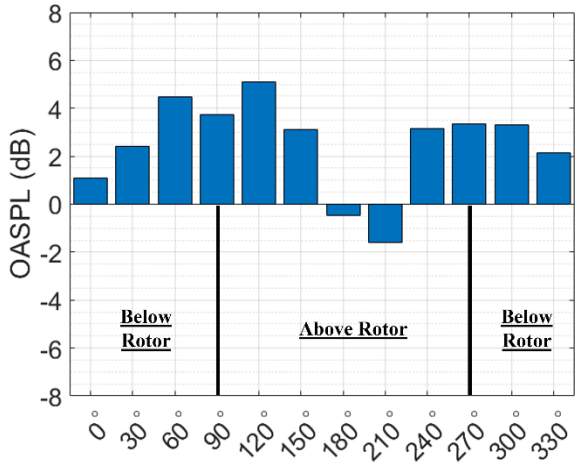

Figure 22 – OASPL difference in vertical plane in wind direction (Interaction – Isolated)

cause a difference in noise when considering bias towards higher frequencies, but this difference is quite small.

The next comparison looks at noise in the wing chord plane, given in Figure 19. Here it is observed that the presence of aerodynamic interactions causes largest increases in loading noise at observers at 120° and 240° in the wing chord plane, on the downstroke side. To get a more quantitative comparison, a difference plot of the noise at observers in 30° increments is given in Figure 20. The noise increase in the wing chord plane is much greater than seen in the rotor plane in Fig. 15, with most observers experiencing a noise increase when aerodynamic interactions are present. The maximum increase is ~7.9 dB at the 120° and 240° observers on the downstroke side. Noise increases in front of the rotor are generally similar to those observed behind the rotor, with the increases to the front of the rotor being only slightly larger. The average noise increase over all observers in the wing chord plane is 3.50 dB.

Next is the comparison of noise in a vertical hub plane in the oncoming wind direction, given in Figure 21. In this plane, the noise difference again is at the front and the rear of the rotor where loading noise is dominant. A comparison of the noise between the isolated rotor and rotor with aerodynamic interactions is given in a difference plot in Figure 22. This comparison shows that the noise increase in the front of the rotor is different depending on if you are above or below the rotor. The noise increases above the rotor are greater than those below the rotor, with the maximum noise increase below the rotor 5.10 dB and the maximum increase above the rotor 4.48 dB. Additionally, the noise increase behind the rotor is greater, with the largest increase behind being 5.10 dB and the greatest increase in front being 3.36 dB. Across all observers, the average increase in noise is 2.49 dB.

This increase in noise on both the wing chord plane and the vertical hub plane in the wind direction is because of the high loading concentration along the bottom of the rotor disk which results in a greater noise in certain directions. Overall, while the presence of wing-induced aerodynamic interactions reduces the total rotor thrust by 3.3%, the increased peak loading and the asymmetry in loading between the top and bottom of the rotor disk causes an increase in the loading noise. Over the three observer planes examined a maximum increase of nearly 8 dB was observed, due to interactional aerodynamic effects (compared to the noise from isolated rotor at the same observer position).

4. CONCLUSION

This study examines the acoustic effects of aerodynamic interactions for two different systems: a two-rotor assembly in cruise and a propeller acting in he presence of a wing. The

two-rotor system examined different disk loadings (6, 8, and 12 lb/ft^2) at a fixed 40 knots cruise speed and different cruise speeds (20, 40, and 60 knots) at a fixed 6 lb/ft^2 disk loading. Loads that captured the aerodynamic interactions between rotors were generated using the commercial CFD solver AcuSolve. The loads were provided to an acoustic propagation model to predict tonal and broadband noise at chosen observers in the rotor plane. The noise generated by the two-rotor pair with aerodynamic interactions was compared to a simulation in which the rear rotor acted in isolation to determine the acoustic effects of the aerodynamic interactions. For the propeller-wing case, the configuration was simulated at 24 knots cruise at 8° AoA. The loads for a rotor in isolation and a rotor acting in the presence of a wing were generated using the commercial CFD solver AcuSolve. The loads were used as inputs for an acoustic solver that predicted noise at observers in the plane of the propeller, the plane of the wing chord, and a vertical plane through the hub in the direction of the wind. Comparisons between the noise produced by the rotor acting in isolation and the rotor acting in the presence of a wing were made to examine how the presence of aerodynamic interactions due to the wing changed the acoustics of the rotor. From these simulations the following conclusions can be drawn:

1. The aerodynamic interactions of a front rotor acting on a rear rotor in cruise do not significantly change the tonal noise of the two-rotor system. For all of the considered loading and cruise conditions, the maximum change in noise due to aerodynamic interactions is 2.1 dB and the greatest absolute average change in noise is 0.6 dB. Additionally, the presence of aerodynamic interactions do not fundamentally change the pressure signal and there is no appreciable difference in the noise at higher frequencies between the isolated and interactional cases.
2. The presence of interactions in a two-rotor system increase the broadband noise. For all considered loading and cruise conditions, the presence of aerodynamic interactions increased the broadband noise at all observers, up to a maximum of 1.85 dB. However, as tonal noise is the dominant noise source, this increase in broadband noise does not result in a change in the overall noise levels.
3. The aerodynamic interactions caused by a wing on a rotor changes the loading noise due to the peak thrust being higher and a significant up-down asymmetry in loading being introduced. In the plane of the rotor this results in an increase in noise of up to 2.23 dB below the rotor and on the upstroke side (Ψ = 330° - 150°) and a reduction in noise of up to 2.17 dB above the rotor and on the downstroke side (Ψ = 225° - 300°), as compared to an isolated rotor. When considering noise in the wing chord plane, the greatest increases in noise are on the downstroke side, almost equally in front of the rotor and behind the rotor, resulting in noise levels almost 8 dB higher than those produced by an isolated rotor at the same observer locations. In a vertical hub plane in the wind direction the maximum increase in noise is up to 5.10 dB (above and behind the rotor).

REFERENCES

1. Swartz, K., "NASA Embraces Urban Air Mobility," Vertiflite Magazine, Jan-Feb 2019.
2. Schmitz, F., "The Challenges and Possibilities of a Truly Quiet Helicopter: 29th Alexander A. Nikolsky Honorary Lecture," *Journal of American Helicopter Society*, Vol. 61, No.4, 2016, pp. 1-33.
3. Zawodny, N., Boyd, D. D., and Burley, C., "Acoustic Characterization and Prediction of Representative, Small-Scale Rotary-Wing Unmanned Aircraft System Components," *72nd Annual Forum of the American Helicopter Society*, West Palm Beach, FL, May 2016.
4. Zawodny, N., and Boyd, D. D., "Investigation of Rotor-Airframe Interaction Noise Associated with Small-Scale Rotary-Wing Unmanned Aircraft Systems," *73rd Annual Forum of the American Helicopter Society*, Fort Worth, TX, May 2017.
5. Pettingill, N. and Zawodny, N., "Identification and Prediction of Broadband Noise for a Small Quadcopter," *75th Annual Forum of the Vertical Flight Society*, Philadelphia, PA, May 2019.
6. Thurman, S. C., Zawodny, S. N., Baeder, D. J., "Computational Prediction of Broadband Noise from a Representative Small Unmanned Aerial System Rotor," *76th Annual Forum of the Vertical Flight Society*, Virtual, 2020.
7. Intaratep, N., Alexander, W., and Devenport, W., "Experimental Study of Quadcopter Acoustics and Performance at Static Thrust Conditions," *22nd AIAA/CEAS Aeroacoustics Conference*, Lyon, France, May 2016.
8. Lee, S. and Shlesigner, I., "Coaxial Rotor Broadband Noise Prediction in Hover", *76th Annual Forum of the Vertical Flight Society*, Virtual, 2020.
9. Jacobellis, G., Singh, R., Johnson, C., Sirohi, J., and McDonald, R., "Experimental and Computational Investigation of Stacked Rotor Acoustics in Hover," *76th Annual Forum of the Vertical Flight Society*, Virtual, 2020.
10. Mankbadi, R. R., Afari, S. O., and Golubev, V. V., "Simulations of Broadband Noise of a Small UAV Propeller," AIAA SciTech 2020 Forum, 6-10 January 2020, Orlando, FL, https://doi.org/10.2514/6.2020-1493.
11. Gandhi, F., Pepe, J., Smith B. (2022). "High Solidity, Low Tip-Speed Rotors for Reduced eVTOL Tonal Noise," *78th Annual Forum of the Vertical Flight Society*, Fort Worth, TX, May 2022.
12. Schiller, N., Pascioni, K., and Zawodny, N., "Tonal Noise Control using Rotor Phase Synchronization," *75th*

Annual Forum of the Vertical Flight Society, Philadelphia, PA, May 2019.

13. Pascioni, K. A., Rizzi, S. A., and Schiller, N.H., "Noise reduction potential of phase control for distributed propulsion vehicles," Paper AIAA 2019-1069, AIAA SciTech Forum and Exposition Proceedings, San Diego, CA, January 2019.
14. Smith, B., Gandhi, F., and Niemiec, R., "A Comparison of Tonal Noise Characteristics of Large Multicopters with Phased Rotors,"*Journal of the American Helicopter Society*, Jan 10, 2023; https://doi.org/10.4050/JAHS.68.032008
15. Smith, B., Gandhi, F., and Lyrintzis, A., "An Assessment of Multicopter Noise in Edgewise Flight," *77th Annual Forum of the Vertical Flight Society*, Virtual, May 2021.
16. Jia, Z., and Lee, S., "Acoustic Analysis of Urban Air Mobility Quadrotor Aircraft," *Vertical Flight Society's Transformative Vertical Flight Forum*, San Jose, CA, Jan 21-23, 2020.
17. Alvarez, J. E., Schenk, A., Critchfield, T., Ning, A., "Rotor-on-Rotor Aeroacoustic Interactions of Multirotor in Hover," 76th Annual Forum of the Vertical Flight Society, Virginia Beach, VA, 2020
18. Zhang, J., Brentner, K., and Smith, E., "Prediction of the Aerodynamic and Acoustic Impact of Propeller-Wing Interference," *Vertical Flight Society's Transformative Vertical Flight Forum*, San Jose, CA, Jan 21-23, 2020.
19. Smith, B., Healy, R., Gandhi, F., and Lyrintzis, A, "eVTOL Rotor Noise in Ground Effect," *77th Annual Forum of the Vertical Flight Society*, Virtual, 2021.
20. Healy, R., Misiorowski, M., and Gandhi, F., "A CFD-Based Examination of Rotor-Rotor Separation Effects on Interactional Aerodynamics for eVTOL Aircraft," *Journal of the American Helicopter Society*, August 2021.
21. M. Misiorowski, F. Gandhi, and A. A. Oberai, "Computational Study on Rotor Interactional Effects for a Quadcopter in Edgewise Flight," *AIAA Journal*, Vol. 57, No. 12, December 2019, pp. 5309-5319; https://doi.org/10.2514/1.J058369.
22. Brentner, K., Bres, G. A., and Perez, G., "Maneuvering Rotorcraft Noise Prediction: A New Code for a New Problem," *AHS Aerodynamics, Acoustics, and Test and Evaluation Technical Specialist Meeting*, San Fransisco, CA, Jan. 2002.
23. Lopes, V. L., and Burley, C. L, "Design of the Next Generation Aircraft Noise Prediction Program: ANOPP2," *17th AIAA/CEAS Aeroacoustics Conference*, Portland, Oregan, June 05-06, 2011.
24. Hebbar, U., Gandhi, F., and Sahni, O., "Parametric Investigation of Flow Over a Rotor-Blown Wing using High-fidelity Simulations," *78th Annual Forum of the American Helicopter Society*, Fort Worth, TX, 2022.
25. Singh, R., Sirohi, J., and Hrishikenvan, V., "Common Research Configuration for Collarborative Advancement of Scalable VTOL UAS Technologies," *75th Annual Forum of the American Helicopter Society*, Philadelphia, PA, May 2019.
26. Russell, C., and Sekula, M., "Comprehensive Analysis Modeling of Small-Scale UAS Rotors," *VFS 76th Forum Annual Forum*, Virtual, 2020.
27. Hebbar, U., Sahni, O., and Gandhi, F., "Comparison of Numerical Modeling Approaches for Flow Over a Wing With an Upstream Rotor," *AIAA Scitech 2022 Forum*, 2022.